Journal of Catalysis 273 (2010) 92–102

Contents lists available at ScienceDirect

Journal of Catalysis

journal homepage: www.elsevier.com/locate/jcat

Interplay between carbon monoxide, hydrides, and carbides in selective alkyne hydrogenation on palladium

Mónica García-Mota [a,1], Blaise Bridier [a,1,2], Javier Pérez-Ramírez [a,b,*], Núria López [a,**]

[a] Institute of Chemical Research of Catalonia (ICIQ), Avinguda dels Països Catalans 16, 43007 Tarragona, Spain
[b] Catalan Institution for Research and Advanced Studies (ICREA), Passeig de Lluís Companys 16, 08020 Barcelona, Spain

ARTICLE INFO

Article history:
Received 15 February 2010
Revised 13 April 2010
Accepted 29 April 2010
Available online 12 June 2010

Keywords:
Palladium
Selective hydrogenation
Alkyne
Alkene
Alkane
Oligomer
Carbide
Carbon monoxide
Hydride
DFT

ABSTRACT

Alkyne hydrogenation, a widely used process in industry to purify olefin streams, comprises a prototype reaction to understand selectivity in heterogeneously catalyzed reactions. The selectivity of the reaction on palladium catalysts to the alkene, alkane, or oligomers strongly depends on the state of the (sub)surface; *i.e.*, the occurrence of complex carbide/hydride phases. In practice, hydrogenation reactors in C2 and C3 cuts of steam crackers require continuous CO feeding in order to enhance the alkene selectivity of palladium-supported catalysts. In the present work, we have studied the impact of carbon monoxide on the formation of carbide and hydride phases as a standpoint to derive structure–performance relationships under realistic process conditions. For this purpose, catalytic tests on a standard 1 wt.% Pd/Al_2O_3 and Density Functional Theory on Pd(1 1 1) were combined. The influence of: (i) the alkyne (ethyne and propyne), (ii) the hydrogen:alkyne ratio (1–10), (iii) the carbon monoxide:hydrogen ratio (0–0.2), and (iv) the catalyst pretreatment on the product distribution was assessed in a continuous flow fixed-bed reactor at ambient pressure. In absence of CO, subtle changes in the hydrogen:alkyne ratio generate undesired products. Carbon monoxide enables the external control of the catalyst state by suppressing the formation of subsurface hydride and carbide phases, thereby stabilizing a high alkene yield in a broad range of feed hydrogen:alkyne ratios. This scenario contrasts with the more fragile regime of the hydride–carbide phases under CO-free conditions. DFT calculations obtained a single Brønsted–Evans–Polanyi relationship independently of the state of the catalyst (carbide, hydride, CO-covered) and the alkyne–alkene–alkane set (C2, C3).

1. Introduction

The focus of catalysis research in the 21st century should be on achieving 100% selectivity for the desired product [1]. This requires sharp chemical transformations, suppressing side paths while being specific to particular functional groups in multi-functionalized molecules or specific to reactants in complex reaction mixtures.

In recent years, partial hydrogenation of alkynes and alkadienes in the presence of alkenes over Pd-based catalysts has been regarded as one of the best playgrounds to identify the control parameters for selectivity [2,3]. This reaction is widely used to upgrade olefin streams by removing highly unsaturated impurities and is carried out over Pd catalysts [4–6]. However, palladium chemistry is extremely sensitive to the presence of subsurface species. On the basis of *in situ* XPS studies, Teschner et al. [2,7] proposed that a substoichiometric carbide phase is responsible for the selectivity towards alkenes. Palladium also forms hydrides, even at low hydrogen pressures [8], which are reported to be unselective [9]. Such subsurface hydrogen species were also reported as very active for nickel [10]. The possible formation of carbide and hydride phases and their relationship with the selectivity of the catalysts has been discussed vividly for several decades [4–6]. It is often perceived in the open literature that the selective character of a certain catalyst in partial alkyne hydrogenation merely is due to the absence of the fully hydrogenated alkane at the reactor outlet. However, in addition to alkene and alkane production, oligomerization has to be taken into consideration. The presence of oligomers (namely C4+ and C6+ products in C2 and C3 hydrogenations, respectively) is known to affect the performance of the catalyst [4]. In fact, the selectivity of pure palladium catalysts is very low, and in practice, promotion by a second metal like Ag or Au and CO feeding are required to increase alkene selectivity [11,12]. In commercial plants, average ethene selectivities of 40%

* Correspondence to: J. Pérez-Ramírez, Institute for Chemical and Bioengineering, Department of chemistry and applied biosciences, ETH Zurich, HCI E125, Wolfgang-Pauli Strasse 10, CH-8093 Zurich, Switzerland.
** Corresponding author.
E-mail addresses: jpr@chem.ethz.ch (J. Pérez-Ramírez), nlopez@iciq.es (N. López).
[1] These authors contributed equally to the results in this manuscript.
[2] Current address: Institute for Chemical and Bioengineering, Department of chemistry and applied biosciences, ETH Zurich, HCI E125, Wolfgang-Pauli Strasse 10, CH-8093 Zurich, Switzerland.

0021-9517/$ - see front matter © 2010 Elsevier Inc. All rights reserved.
doi:10.1016/j.jcat.2010.04.018

have been reported in ethyne hydrogenation over promoted Pd/SiO_2 [13].

As for more recent studies, the reaction pathway for hydrogenation has been studied on pure Pd surfaces [3,14–16], gold nanoparticles [17], copper and nickel surfaces [18,19], and Pd–Ag alloys [20]. In some of these studies [3,16], the thermodynamic factor (*i.e.*, strong adsorption for alkynes and none for alkenes) was identified as the selectivity indicator, while the ability to form C–C bonds (oligomers) was neglected. By optimization of the thermodynamic selectivity factor, a new selective NiZn alloy was identified computationally [3]. Ethyne hydrogenation tests on $NiZn/MgAlO_2$ confirmed that over-hydrogenation to ethane was suppressed. However, in theoretical models, the presence of carbide, hydrides, and selectivity modulators has been addressed only partially. A thermodynamic study of carbide formation was carried out by Teschner et al. [7] showing the dependence on the alkyne nature, C2 vs. C3. In addition, the ethyne–ethene thermodynamic factors for PdC_x ($x = 0.25$–1 ML) and $PdH_{0.5}$ were calculated [16], indicating that carbon lowers the binding energies of unsaturated pairs and that the values for $PdH_{0.5}$ are very similar to those for clean Pd. However, the complete reaction path on the carbide or hydride phases was not performed. As for CO, its positive effect on the thermodynamic factor has been reported recently for the clean surface [21]. CO reduces the size of the available Pd ensembles on the surface and inhibits C–C bond formation from the hydrocarbons. The interplay between CO with carbides and hydrides was not investigated.

In order to understand the selectivity of the industrial process, the overall complexity of the catalytic system under realistic experimental conditions needs to be considered. Thus, both carbide and hydride phases and selectivity enhancers (CO) should be taken into account. In addition, for any rational catalyst design, structure–selectivity relationships must be determined as close as possible to the real conditions.

The aim of the present paper is to establish new structure–selectivity relationships for alkyne hydrogenation on palladium catalysts based on the detailed knowledge of the state of the material under reaction conditions, with or without CO, considering all reactants and products: alkynes, alkenes, alkanes, and oligomers. To achieve this goal, the partial hydrogenation of ethyne and propyne was studied by means of systematic catalytic tests over a standard 1 wt.% Pd/Al_2O_3 and Density Functional Theory, DFT. In both cases, different initial states of the catalyst were investigated.

2. Catalytic tests

Catalytic tests were carried out over a 1 wt.% Pd/γ-Al_2O_3 (Aldrich, ref: 20,570–2). N_2 adsorption at 77 K was measured in a Quantachrome Autosorb-1MP analyzer. Prior to the analysis, the sample was degassed at 373 K for 16 h. Pd dispersion was determined by CO chemisorption using a volumetric apparatus (Quantachrome Autosorb-1C). Prior to CO chemisorption, the sample was heated in He at 573 K (5 K min^{-1}) for 30 min, reduced in H_2 (50 cm^3 min^{-1}) at 473 K for 2 h (3 K min^{-1}), evacuated at 473 K for 2 h, and cooled down to 308 K in vacuum. Based on the amount of CO adsorbed and assuming an adsorption stoichiometry CO:Pd = 1:1, the metal dispersion was calculated.

The gas-phase hydrogenation of ethyne and propyne was studied at a total pressure of 1 bar and 348 K in a MicroActivity Reference set up (PID Eng&Tech). The catalyst (0.15 g, sieve fraction 200–400 μm) was loaded in the quartz microreactor (12 mm i.d.) and heated in He (42 cm^3 min^{-1}) at 573 K (5 K min^{-1}) for 30 min before each reaction. Three types of tests were carried out:

(i) Influence of the H_2:alkyne ratio (1–10): the inlet alkyne concentration was kept at 2.5 vol.%, and the inlet H_2 concentration was increased from 2.5 to 25 vol.% every 2 h. This set of experiments was repeated with an inlet CO concentration of 0.1 vol.%.

(ii) Influence of the CO:H_2 ratio (0–0.2): the inlet alkyne and hydrogen concentrations were kept at 2.5 vol.% and 12.5 vol.%, respectively (H_2:alkyne = 5), and the CO concentration was gradually increased from 0 to 2.5 vol.% every 2 h.

(iii) Influence of the pretreatment in the absence or presence of carbon monoxide. The catalyst was tested without pretreatment (besides the drying step in He at 573 K) or after pretreatment in (a) 2.5 vol.% alkyne in He, (b) 5 vol.% H_2 in He, and (c) 2.5 vol.% alkyne and 3.75 vol.% H_2 in He (reaction mixture). The pretreatments were carried out at 473 K for 30 min using a total gas flow of 42 cm^3 min^{-1}. Afterwards, the catalyst was cooled down in the same gas mixture to 348 K (5 K min^{-1}) and evaluated in two feed mixtures: alkyne:H_2:He = 2.5:3.75:93.75 and alkyne:CO:H_2:He = 2.5:0.1:3.75:93.65.

In the catalytic tests, the total flow was kept constant at 42 cm^3 min^{-1} (space velocity, SV = 16,800 cm^3 h^{-1} g^{-1}) by balancing the mixtures with He. Fresh catalyst was loaded in each test and for each pretreatment. The plotted values in the graphs along the article correspond to a reaction time of 2 h. Stable values of conversion and selectivity were typically achieved in 30 min after a change in reaction conditions. Therefore, data at 2 h can be safely considered as the steady state. Alkynes, alkenes, and alkanes were analyzed by a gas chromatograph (Agilent GC6890N) equipped with a GS-GasPro column and a thermal conductivity detector. The selectivity to the alkene (alkane) was determined as the amount of alkene (alkane) formed divided by the amount of reacted alkyne. The selectivity to oligomers was obtained as: S(oligomers) = 1 − S(alkene) − S(alkane).

It should be mentioned that, for simplification purposes, neither the catalyst nor the experimental conditions matched what is used for industrial alkyne hydrogenation. 1 wt.% Pd/γ-Al_2O_3 is a commercially available palladium-supported catalyst, while the catalyst installed in plants (i) has a much lower Pd content, (ii) eggshell Pd distribution, (iii) non-acidic support, and (iv) contains metal promoters. Besides, we conducted catalytic tests at 1 bar while the service pressure in gas-phase ethyne and propyne hydrogenation in industrial reactors is around 20 bar [6]. These simplifications are not expected to qualitatively change the dependence of the product distribution on the variables studied (H_2:alkyne and CO:H_2 ratios, catalyst pretreatment).

3. Computational techniques

The catalytic hydrogenation of ethyne and propyne was studied by means of periodic Density Functional Theory (DFT) applied to slabs and calculated with the VASP code [22]. The Pd cell parameter was 3.966 Å in agreement with the experimentally determined [23]. We employed the lowest surface energy facet (1 1 1) to describe the alkyne hydrogenation activity since this surface is the most common for fcc metals. The (1 1 1) slabs consist on four atomic layers and a $p(2 \times 2)$ reconstruction. Four different models were set up: (i) clean Pd surface, (ii) a near-surface carbide (carbon content 0.25 ML), (iii) a fully hydrogenated Pd system, and (iv) a partially CO-covered surface (CO coverage 0.25 ML) (see Supplementary material S1 for a schematic representation). As we will see later, the CO coverage employed might be low in terms of the real CO population on the surface. However, the present set up allows enough empty space for the reactions to take place. To

study C–C coupling reactions (oligomerization), we have used a larger supercell $p(2 \times 4)$ where two alkyne molecules have been placed, thus keeping the same hydrocarbon coverage employed in the hydrogenation steps. Different C–C couplings: between an alkyne and CO, between two alkynes, and between an alkyne and a partially hydrogenated moiety have been investigated. This allows us to explore the incorporation of CO to the oligomers as proposed by Borodzinski and Bond [24]. *k*-point meshes of $5 \times 5 \times 1$ were considered for the $p(2 \times 2)$ cell and reduced to $5 \times 3 \times 1$ for the $p(2 \times 4)$ cell [25]. The energy profiles were studied with the GGA-PW91 functional [26]. In the calculations, inner electrons were represented by PAW pseudopotentials [27], and the monoelectronic valence states were expanded with plane waves with kinetic energies lower than 400 eV. Transition states were located by the Climbing Image version of the Nudged Elastic Band, CI-NEB, method [28] and were proven to show a single imaginary frequency.

To obtain the chemical state of the surface under different environments, the above-described $p(2 \times 2)$ supercell was employed. In that case, sequential hydrogen additions, first to the surface layer and then to subsequent layers, were introduced, following the procedure by Mavrikakis et al. [29] To model the hydride phase, lattice enlargements were taken into account as it corresponds to the experimental observation for the β-PdH phase [8]. Since the description in energy terms does not account for the effect of temperatures and pressures in hydride formation, first-principle thermodynamics were employed to obtain Gibbs energies. Hydride formation in Pd can be understood as a particular case of multilayered adsorption [30], the final equation being:

$$V/V_m = \sum_{i=0}^{\infty} i\theta_i \Big/ \sum_{i=0}^{\infty} \theta_i = cx/[(1-x)(1+(c-1)x)] \quad (1)$$

where V/V_m represents the number *i* of H-multilayers adsorbed, and *c* and *x* are related to the partial hydrogen pressure and adsorption–desorption constants of the surface layer k_1, k_{-1}; or the resting layers *k*, k_-; then $c = (k_1\ p_{H2}/k_{-1})^{1/2}/x$ and $x = (k\ p_{H2}/k_-)^{1/2}$, and p_{H2} stands for the hydrogen pressure. If some carbon, alkyne, or CO impurities are present then the equation is modified and reads as follows:

$$\begin{aligned} V/V_m = {} & [cx + 6(1-x)^2 K_C (p_{C2H2}/p_{H2})^{1/2} f_H \\ & + 2(1-x)^2 K_{C2H2} p_{C2H2} f_H]/[(1-x)(cx + 7(1-x) \\ & \times K_C (p_{C2H2}/p_{H2})^{1/2} + 3(1-x) K_{C2H2} p_{C2H2})] \end{aligned} \quad (2)$$

$$V/V_m = cx/[(1-x)((1-x) + cx + (1-x)K_{CO} p_{CO})] \quad (3)$$

where K_C is the formation constant of the carbide, and K_{C2H2}, and K_{CO} are the adsorption constants of C_2H_2, and CO, respectively; and p_{C2H2} and p_{CO} their corresponding partial pressures and f_H the filling factor of the areas close to carbide and ethyne. Full derivation of these equations is elaborated in the Supplementary material.

4. Results and discussion

In the following section, we first describe the effect of the hydrogen:alkyne ratio in order to analyze the role of carbide and hydride formation. In this analysis, the reaction network for three systems has been considered: clean surface, carbide-containing, and hydride-containing. Finally, the role of carbon monoxide in the balance between carbide and hydride, and the barriers are taken into account for both the clean and CO-covered surface.

4.1. Catalytic performance

The total surface area of the 1 wt.%. Pd/Al_2O_3 sample (S_{BET}) was 210 $m^2\ g^{-1}$. CO chemisorption revealed a Pd dispersion in the catalyst of 22%, yielding an average Pd particle size of 5 nm (assuming hemispherical particle). Alkyne hydrogenation tests assessed the influence of the H_2:alkyne ratio and the CO:H_2 ratio on the product distribution. Besides, the impact of the catalyst pretreatment on the CO effect was evaluated. All tests were systematically conducted with ethyne and propyne in order to extrapolate conclusions to relevant substrates with different carbon number. Few studies in the literature include both alkynes, and since the catalyst, reaction conditions, and reactor configurations employed differ substantially, a proper comparison of catalytic data is sometimes not straightforward. The different scenarios studied experimentally are compared with complementary computational results in the next section.

4.1.1. H_2:alkyne ratio

Fig. 1 shows that the alkyne conversion at 348 K was complete at all H_2:alkyne ratios, except for values around 90% for both alkynes at the stoichiometric ratio of 1. The selectivity to ethene and propene with H_2:alkyne = 1 was 42% and 62%, respectively. These values decrease steadily upon increasing the inlet partial H_2 pressure. The same trend described for the selectivity to the olefin was followed by the selectivity to oligomers, starting at *ca.* 30–40% with H_2:alkyne = 1. The selectivity to the alkane exhibited an opposite trend, increasing from 10% to 20% at H_2:alkyne = 1 to 80–90% at H_2:alkyne = 10. At H_2:alkyne > 4, the selectivity to products remained essentially constant: no alkene production and *ca.* 90% to the fully hydrogenated alkane but still the selectivity to oligomers amounted to *ca.* 10%. The low alkene selectivity of unpromoted palladium catalysts has been stressed by various authors [11,12]; addition of a second metal (Ag) or continuous feeding of carbon monoxide is mandatory to explain its successful implementation in industry (*vide infra*). The loss of alkene selectivity upon increasing the H_2:alkyne ratios has been typically explained by the formation of the β-PdH phase, which is selective to the over-hydrogenated product [4,9]. In qualitative terms, the dependencies of the product distribution on the H_2:alkyne ratio were very similar for C2 and C3. More specifically, it can be observed that at low H_2:alkyne ratios, the selectivity to propene is higher than to ethene by more than 10%. This difference smoothed out when increasing the inlet partial H_2 pressure. The selectivity to the alkane was higher for C2 than for C3 at all H_2:alkyne ratios. In

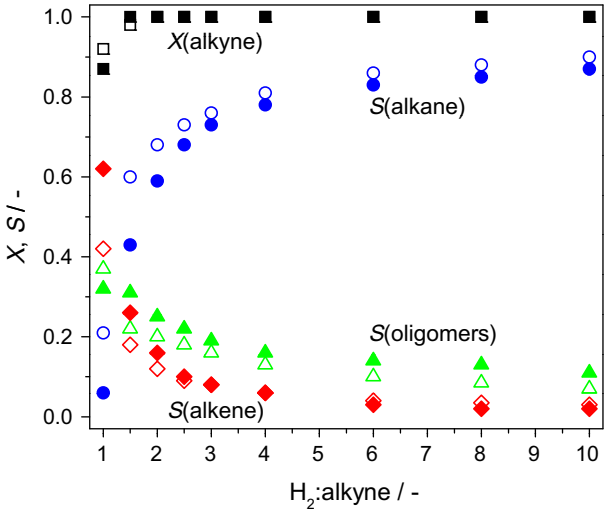

Fig. 1. Conversion (*X*) of ethyne (propyne) and selectivity (*S*) to the alkene, alkane, and oligomers over Pd/Al_2O_3 as a function of the H_2:alkyne ratio. Ethyne (propyne) and the derived products are represented by open (solid) symbols. Conditions: *T* = 348 K, *SV* = 16,800 $cm^3\ g^{-1}\ h^{-1}$, and *P* = 1 bar.

any case, the main outcome from Fig. 1 is that, oligomerization is the most competitive path under H-lean conditions (hydrogen:alkyne $\leqslant 1$), whereas at hydrogen:alkyne $\geqslant 2$ the alkane in the main product. The ratio of 1.5–1.7 corresponds to a switch for alkene:alkane selectivity. Indeed, the narrow window under which selective hydrogenation is observed on palladium stresses the major role of surface modifiers in the industrial process.

4.1.2. H_2:CO ratio

The increase in alkene selectivity upon addition of carbon monoxide has been demonstrated in the past; this effect is reversible, *i.e.*, it disappears when CO feeding is turned off [4,9]. The influence of CO on the production of oligomers has been assessed in a less systematic way, and there are contradictory statements [24]: some authors said that CO reduces the selectivity to green oil while others indicated that CO leads to the occurrence of more carbon deposits. In our experiments, the influence of CO as selectivity enhancer was studied in two different regimes. First, the H_2:alkyne ratio was set to five while gradually increasing the CO:H_2 ratio (Fig. 2). The selected H_2:alkyne ratio in the feed was relatively high in order to evidence more clearly the decrease in alkane production upon CO addition. Addition of very low amounts of carbon monoxide (CO:H_2 < 0.002) led to a marked decrease in the alkane selectivity at the expense of an increased production of the alkene and oligomers. A further increase in the inlet partial CO pressure (CO:H_2 = 0.04) completely suppressed over-hydrogenation and led to a maximum alkene selectivity (*ca.* 30% ethene and *ca.* 60% propene), see Fig. 2. Within this range of CO:H_2 ratios ($\leqslant$0.04), the degree of alkyne conversion was >90%. Excess of carbon monoxide (CO:H_2 > 0.1) was detrimental, lowering the alkyne conversion (down to 30%) and alkene selectivity (*ca.* 20% ethene *and ca.* 30% propene). The pathway to the alkane was suppressed, and oligomers are the major by-product, reaching a selectivity of *ca.* 85% for C2 and *ca.* 75% for C3. Therefore, CO acts a external switch of the alkene:alkane:oligomers distribution and, by optimization, it enables to adjust the partial hydrogenation depending on the inlet H_2:alkyne ratio. The yield of alkene/oligomers, determined as the product of alkyne conversion and alkene/oligomer selectivity, is presented in Fig. 3. The alkene yield presents a maximum in the range 0.02–0.04, which allows a pretty wide operating window.

In the second set of experiments, a constant CO content of 0.1 vol.% was employed while the H_2:C_3H_4 ratio was varied between 1 and 10. The effect of the feed hydrogen-to-propyne ratio on the propyne conversion and selectivity to products is presented in Fig. 4. The product distributions over clean Pd and in the presence of CO were markedly different. Partial hydrogenation of propyne in the presence of CO was hardly affected by the inlet partial H_2 pressure, in contrast with the results discussed in the previous section for Pd. The selectivity to propene at very low H_2:C_3H_4 ratios was relatively low (46%) in favor of a higher selectivity to oligomers (54%). In the other extreme, *i.e.*, at very high H_2:C_3H_4 ratios, the selectivity to propene was still remarkably high *ca.* 70%, and only little propane was produced (3%). For H_2:C_3H_4 ratios in the range of 2–10, the selectivity to alkene was within the range of 60–70%, to oligomers 30–40% and that to the alkane virtually zero. Propyne conversion was practically complete at any ratio.

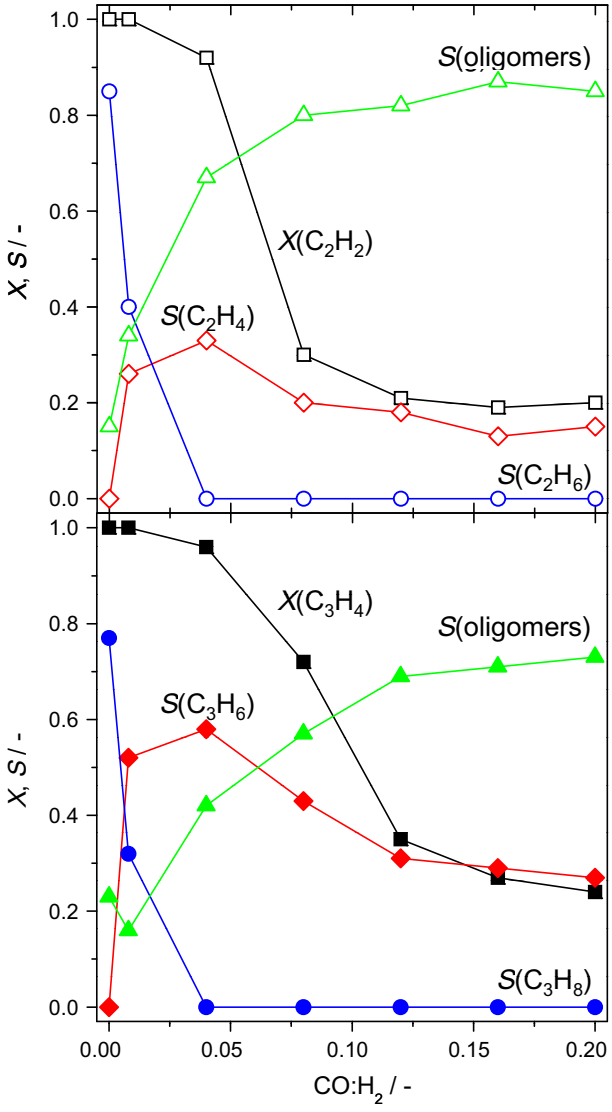

Fig. 2. Conversion (X) of ethyne and propyne and selectivity (S) to the alkene, alkane, and oligomers over Pd/Al_2O_3 as a function of the CO:H_2 ratio. Ethyne (propyne) and the derived products are represented by open (solid) symbols. Conditions: H_2:alkyne = 5, T = 348 K, SV = 16,800 $cm^3\ g^{-1}\ h^{-1}$, and P = 1 bar.

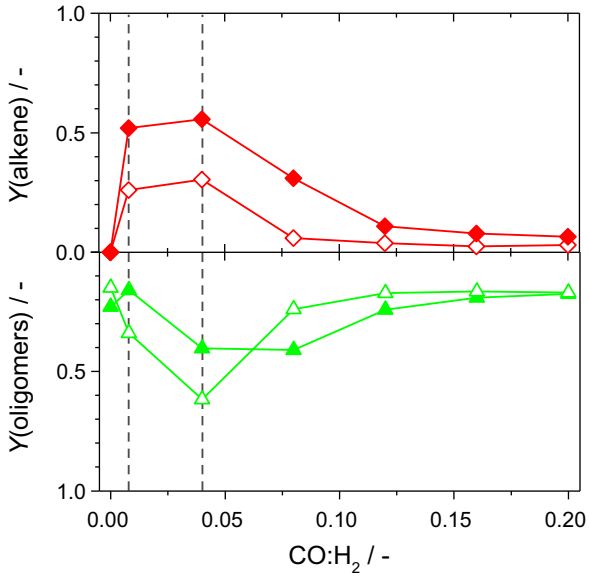

Fig. 3. Dependence of the yield of alkene and oligomers on the CO:H_2 ratio. The yield was determined as the product of alkyne conversion and product selectivity given in Fig. 2. (◇, △) represent the C2 values and (♦, ▲) the C3 ones.

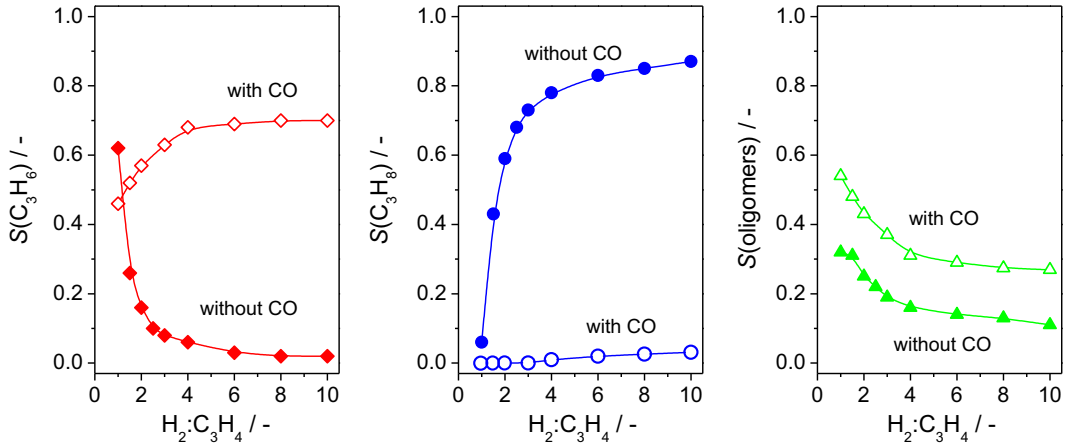

Fig. 4. Selectivity to propene (♦, ◇), propane (●, ○), and oligomers (▲, △) as a function of the H_2:propyne ratio over Pd/Al_2O_3 in the absence (solid symbol) or presence of CO (open symbol). Conditions: 2.5 vol.% propyne, 2.5–25 vol.% H_2, and 0 or 0.1 vol.% CO, balance He, T = 348 K, SV = 16,800 $cm^3\ g^{-1}\ h^{-1}$, and P = 1 bar.

4.1.3. Pretreatment

A third type of experiments was dedicated to study the influence of CO on alkyne hydrogenation over differently pretreated catalysts (Fig. 5). The pretreatment conditions influence the state of palladium (clean, H-rich and C-containing) prior to reaction. For ethyne and the non-pretreated catalyst, CO addition lowers the conversion, suppresses ethane production, and increases both the ethene and oligomer selectivity. When the catalyst was pretreated in ethyne, ethene selectivity did not change upon CO addition, and the oligomer selectivity increased at the expense of ethane. When the sample was exposed to high partial H_2 pressure, the alkyne conversion was high, and the alkane was the major product (75% selectivity), the second product being oligomers (24% selectivity), and minor ethene production. If CO was added, ethyne conversion decreased, then the major products were oligomers, ethene production was enhanced, and the complete quenching of ethane was observed. When the catalyst was pretreated under reaction mixture, the effect of CO addition was very similar to the results observed for non-pretreated catalyst.

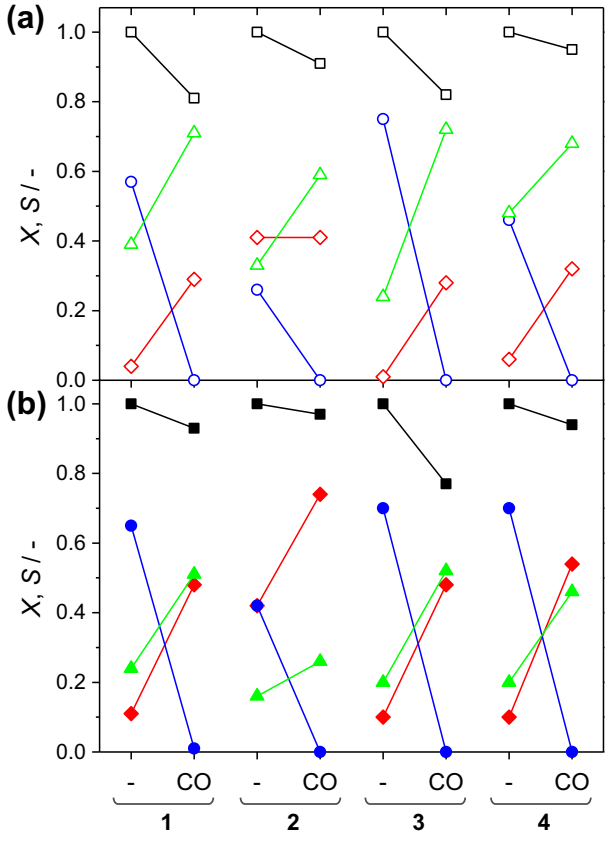

Fig. 5. Influence of the pretreatment of Pd/Al_2O_3 on the hydrogenation of ethyne ((a), open symbols) and propyne ((b), solid symbols) in the absence or presence of CO. Symbols: (□, ■) alkyne conversion, (◇, ♦) alkene selectivity, (○, ●) alkane selectivity, and (△,▲) selectivity to oligomers. Pretreatments: (1) no pretreatment, (2) alkyne, (3) H_2, and (4) alkyne + H_2. Conditions: H_2:alkyne = 1.5, CO:H_2 = 0 or 0.03, T = 348 K, SV = 16,800 $cm^3\ g^{-1}\ h^{-1}$, and P = 1 bar.

The results for C3 parallel those of C2. The main differences observed were for C3, alkene was more likely to appear both in presence and in absence of CO, which points out to the intrinsic properties of the unsaturated C3 when compared to the C2 counterparts in terms of oligomerization. Oligomeric compounds were more likely to be formed with C2 (*ca.* 40% for C2 compared to *ca.* 20% for C3). The most striking difference appeared in regard to alkyne pretreatment. In both cases, this led to more selective alkene catalysts, while the introduction of CO in the feed resulted in no change in alkene selectivity in the case of C2, and a large increase (about 30%) for C3.

To sum up, upon CO addition, alkyne conversion decreased by 10–20%. Under hydrocarbon pretreatment, alkenes were the major product, and the presence of CO improved alkene production in the case of C3. The effect of CO was much more important in the case of hydrogen pretreatment where initially over-hydrogenated products predominated (selectivity ~70%). CO blocked this process but did not completely suppress it in the case of C2. Nevertheless, after hydrogen pretreatment, CO addition improved the selectivity to the double bond even if the effect was more significant in propyne hydrogenation. Finally, if the pretreatment was carried out under reaction conditions, the hydrogenation behavior of C2 and C3 was similar to the one observed over non-pretreated catalyst: oligomers and the alkane were obtained for C2, while the alkane was the major product for C3. After CO addition, alkene production was enhanced but the olefin was the major product only for C3.

4.2. States of the system

By extensive use of DFT-based simulations, the interplay between the carbide, hydride, and CO-rich phases was analyzed employing models similar to those in first-principle thermodynamics [31].

4.2.1. Hydride formation

The formation of hydrides and carbides has been proposed and documented under some conditions in the past [5,9]. PdH_x shows both a low-H-content α-$PdH_{0.02}$ phase, and a high content β-$PdH_{0.7}$ phase [8]. From our models, starting with the clean Pd(1 1 1) surface, hydrogen is adsorbed exothermically, by 0.58 eV/H atom, at 0.25 ML coverage. H_2 dissociation is easy even at a high hydrogen coverage [32,33]. The average adsorption energies per atom for the clean surface at full hydrogen coverage (1 ML) are close to −0.5 eV/surface H atom and much smaller for the inner octahedral sites, around −0.1 eV/bulk H atom. The low dissociation barrier of H_2 and the easy incorporation along (1 1 1) surfaces indicate that the entire surface can capture and incorporate H_2.

4.2.2. Carbide formation

Carbide formation arises from the decomposition of organic moieties [34,35]. According to Andersin et al. [36], ethene dissociation into two methylene groups is hindered by a barrier of 2.12 eV barrier on the Pd(1 1 1) surface, but it is reduced to 1.69 eV at the step. Therefore, formation of C-related species takes place mainly at steps. In fact, the adsorption energy of C atoms (with respect to gas-phase C_2H_2 and H_2) is exothermic by 1.0 eV at the step (endothermic by 0.2 eV with respect to C_2H_4 and H_2). The formation of the C-containing deposits strongly depends on the chemical potential of the alkyne–alkene pairs as reported by Teschner et al. [7] and corroborated by us in the Supplementary material. Once carbon atoms are formed they can diffuse inside the step to the near-surface layer [37]. From our calculations, the process is hindered by a barrier between 0.8 and 1.0 eV depending on the coverage (0.33 or 0.17 ML C atoms at the step). This agrees with the experimental observations in the group of Kiwi-Minsker, which attributed the formation of a carbide layer near defective sites to the low turn-over frequency found for small particles when compared to larger ones [38].

The binding energy of the carbide at low coverages (0.0625 ML) is similar to the value at the step (about 1 eV with respect to gas-phase C_2H_2 and H_2). Diffusion in the near-surface layer is rather easy, the activation energy for diffusion being $E_{a,\text{diffusion}} = 0.71$ eV. This value is in agreement with the 0.72 eV estimate from STM experiments for the denominated β-impurities and with previous computational results [34,35]. The carbide phase is not very dense in C atoms, as C insertion close to a near-subsurface carbon position is repulsive by 0.6 eV at neighboring sites (0.1 eV at second next nearest neighbors). This is compatible with the $PdC_{0.15}$ phase reported by Ziemecki et al. [39] The most favorable positions for C atoms in Pd are the octahedral subsurface sites; penetration towards the bulk has a thermodynamic penalty cost of 0.04 eV for the subsurface layer (and more than 1.5 eV for bulk Pd). The reason for near-surface carbide formation is closely related to the higher *d*-band energy of the Pd atoms on the surface and to the fact that geometric relaxations are also easier for surface atoms than for bulk atoms. From the previous data, the near-surface positions close to the step edges are most likely *poisoned* by the formation of the carbide, the extension of the carbide depends on the diffusion from these positions towards the center of the palladium particle.

4.2.3. Carbide–hydride interplay

To analyze the interplay between the carbide and the hydride phase, we started by a configuration in which a near-subsurface C atom was already present. Adsorption of H atoms on the surface takes place normally. There is an exception for the position on top of the carbon atom where adsorption is not favored. The average adsorption energy of the first H-layer is slightly reduced to −0.46 eV/H atom (−0.58 eV/atom for clean Pd). The insertion of H atoms in the second layer is largely hampered as shown in Fig. 6, and the presence of C in the near-surface layer impedes additional H adsorption even at distances as long as 5 Å (about two positions in the lattice). Thus, H adsorption close to C atoms is less stable than on the surface or in a subsurface layer far away from the C position. For H in the third layer, Pd atoms screen more effectively the presence of C and already at 4 Å (more than one lattice position), the standard value for subsurface H adsorption is retrieved (−0.1 eV/atom). On the other hand, if the initial situation consists on the PdH form, less available step sites for hydrocarbon dissociation exist, thus hampering the formation of carbide. Indeed, C incorporation to the near-surface layer at the step site and under high hydrogen content results in very endothermic insertion, >1.5 eV. Thus, the hydride prevents the formation of carbide layer both by blocking possible carbide positions and by increasing the thermodynamic requirements for insertion.

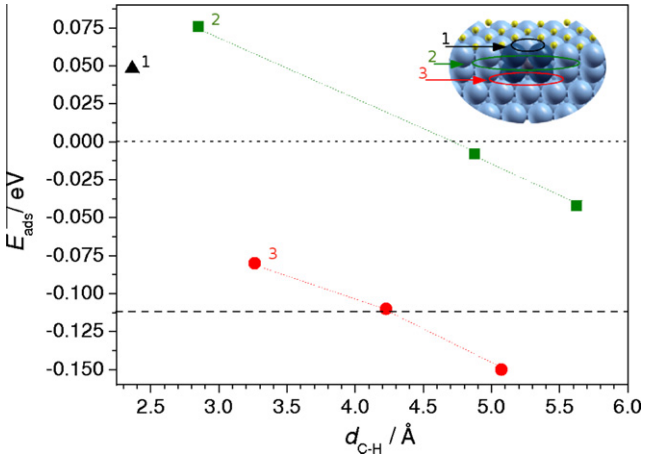

Fig. 6. Adsorption energy of hydrogen, E_{ads} in eV, with respect to gas-phase hydrogen to a palladium carbide model system covered by a H monolayer as a function of the distance between the incoming H and C. Position 1 stands for the surface (▲), position 2 for the subsurface (■), and position 3 for the sub-subsurface (●). The horizontal dashed line indicates the average adsorption energy for subsurface H in clean Pd.

4.2.4. CO-containing systems

CO is known to adsorb on Pd(1 1 1) forming very dense layers even at low partial pressures [40–42]. At low coverage, 0.25 ML, the calculated CO adsorption energy with the present set up is −2.06 eV, which is in close agreement with previous calculations [40]. Dense structures up to $p(2 \times 2) - 3CO$ are usually formed under UHV conditions. For this case, the average CO adsorption energy decreases to −1.43 eV/CO. At 0.25 ML CO coverage, the H binding energies are −0.40 eV/H atom on the surface and even more reduced for subsurface H, *ca.* −0.05 eV. Thus, the formation of a dense CO layer implies the reduction in the number of adsorption sites for H_2 and the decrease in the average binding energies.

Since CO is very strongly bound to the surface, it can interact with carbon impurities, as suggested by Salmeron et al. [34] For instance, in a $p(2 \times 2)$ lattice containing subsurface C, the average CO adsorption energy in the compact 3CO layer is still favorable, −1.16 eV/CO. Moreover, the dense CO layer can cause the carbon atom to penetrate deeper in the Pd structure, since this structure is 0.80 eV more favorable than the corresponding near-surface C. Thus, the CO modifier moves the carbide layer to deeper positions in the Pd particle. This is a dynamic effect since once CO is removed; the diffusion of carbide towards the near-surface position is energetically favored. On the contrary, if the CO layer is deposited first, it blocks the sites at the steps (CO binding energy is −2.11 eV) and impedes the formation of the carbide from alkynes.

The C–CO steady state would then depend both on the history of the sample and on the partial CO pressure.

4.3. Reaction mechanism and kinetics

In the present work, we have carried out a systematic study on the effect of the catalyst state on the reaction network for both the clean Pd surface or in the presence of carbide, hydride, and CO. A complete reaction list with thermodynamic and kinetic parameters is collected in the Supplementary material. Only the most relevant data will be discussed hereafter. Fig. 7 shows the reaction network for the hydrogenation. Parallel paths including oligomer formation and the participation of CO in the oligomerization process will be described too. However, the extensive number of different moieties that can undergo C–C bond formation prevents from carrying out a quantitative analysis of the complex oligomerization reactions.

4.3.1. Hydrogenation

The complete reaction network starts by H_2 dissociation and the adsorption of the alkyne on the surface. Both steps are exothermic under all conditions (clean, C, H, and CO). Then, the sequential addition of H following a Horiuti–Polanyi mechanism [43] can take place. Given the symmetric nature of ethyne, the first hydrogenation leads to a single product vinyl, $HCCH_2$. Vinyl is a branching point intermediate since upon hydrogenation two competitive products, ethene (H_2CCH_2) or ethylidene ($HCCH_3$), can be formed. From H_2CCH_2 or $HCCH_3$, further hydrogenation leads to a common intermediate ethyl, (H_2CCH_3), and finally the fourth hydrogenation leads to ethane. For higher hydrocarbons such as C3, the number of possibilities grows and three branching points exist in the complete hydrogenation path. The complexity of the bifurcation points has not been considered in the majority of the hydrogenation calculations [3], but as we will show later, all these possibilities cannot be *a priori* neglected from an energy point of view and might be the main hydrogenation path for some of catalyst states.

Analyzing the data for the clean surface during ethyne hydrogenation, its adsorption is exothermic by *ca.* 2 eV, the first hydrogenation is exothermic by 0.17 eV, and the barrier is 0.66 eV. The second hydrogenation to ethene shows a barrier of 0.81 eV, while the barrier to ethylidene is 0.79 eV. Both products are more stable than the vinyl intermediate by 0.42 eV for ethene and 0.12 eV for ethylidene. Then, ethene can desorb from the surface, the desorption energy is 0.82 eV. The third hydrogen addition towards ethyl has barriers of 0.74 eV (from H_2CCH_2) and 0.80 eV (from $HCCH_3$), and the final step is hindered by the lowest barrier (0.48 eV) in the hydrogenation process. Summarizing the results: on the clean surface, formation of ethene and ethylidene is almost equally likely, and ethene can either desorb or be further hydrogenated. Thus, both effects are responsible for the relatively low selectivity towards ethene observed for clean Pd. Indeed, our catalytic tests on the non-pretreated Pd/Al_2O_3 catalyst lead to selectivities of 40% (20%) to ethene (ethane) at stoichiometric ratios.

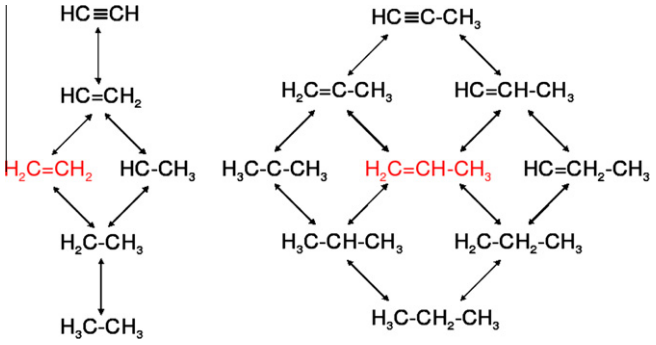

Fig. 7. Reaction network for hydrogenation of ethyne (left) and propyne (right).

Therefore, both binding energies of ethyne and ethene pair (thermodynamic factor) (Table 1) and activation energies of the first branching reaction are crucial to understand selectivity in alkyne hydrogenation. Thermodynamic factors are known to depend on the nature of the catalyst [3,17,21], but also kinetic contributions depend on the nature of the system. For instance, if C is present, the second hydrogenation barriers are 0.57 and 0.69 eV to H_2CCH_2 and $HCCH_3$, respectively. Therefore, the presence of the carbide induces selectivity, both by destabilizing ethene adsorbed on the surface ($E_{ads} = -0.67$ eV to be compared to -0.82 eV for the clean surface) and by improving the second hydrogenation branching ratio. Our results explain the observations of Teschner et al. [2] of improved alkene selectivity in the presence of the carbide phase. If CO is present, the second hydrogenation barriers are 0.88 and 0.57 eV at low CO coverage (0.25 ML), but already at 0.50 ML CO the barriers are reduced to 0.14 and 0.23 eV (ethene and ethylidene), leading to selective ethene production.

The situation is far more complex in the presence of the hydride phase. The first hydrogenation takes place from one of the hydrogen atoms on the surface. This leaves a H-vacancy on the Pd surface with a H in the near-surface position. This nascent hydrogen atom has a chemical potential that exceeds the surface hydrogen atom by 0.45 eV. Thus, once vinyl is formed two options can be triggered, either from a H sitting on the surface (to attack the HC fragment) or from an almost free H atom ($H_{subsurface}$), closer to the CH_2 moiety, see Fig. 8. The corresponding hydrogenation barriers are 0.36 and 0.06 eV, respectively. As a consequence, under these conditions, the major product is ethylidene, and the final product is ethane. This differs from the previous theoretical estimation where the presence of subsurface hydrogen was reported to induce almost no change in the barriers [14], although in that study the direct effect of emerging H atoms was not considered. Therefore, in the case of the hydride, the alkane production is controlled by the opening of surface H-vacancies generated by the first H transfer and the subsequent ejection of the near-surface H.

In the case of C3 hydrogenation, adsorption of propyne on the clean surface is exothermic by 1.57 eV. Then, the first hydrogenation can take place on the primary or secondary carbons, both barriers are about $E_a = 0.70$ eV. From each hydrogen addition, a branching point occurs that leads to the formation of CH_3CH_2CH and propene or to propene and CH_3CCH_3, where the corresponding barriers are 0.72, 0.71, 0.76, and 0.48 eV, respectively. Propene desorption is endothermic by 0.60 eV. Further, propene hydrogenation to $CH_3CH_2CH_2$ or CH_3CHCH_3 is hindered by 0.75 and 0.83 eV barriers. Thus, the competition between propene desorption and further hydrogenation is more favorable towards desorption than for the C2 counterpart. Therefore, propyne hydrogenation is intrinsically more selective to the alkene than ethyne hydrogenation. Any other hydrogenation from the rest of the intermediates in Fig. 7 shows hydrogenation barriers between 0.93 and 0.48 eV. The effects of carbide, CO, and hydrides parallel those found in the description of C2.

Table 1
Adsorption energies, E_{ads} in eV, and differential binding energy, ΔE_{ads} in eV, $\Delta E_{ads} = E_{ads}(\text{alkyne}) - E_{ads}(\text{alkene})$ for C2 and C3 alkynes and alkenes.

	Clean	Carbide	Hydride	CO-covered
$E_{ads}(C_2H_2)$	−2.02	−1.49	−0.94	−1.24
$E_{ads}(C_2H_4)$	−0.82	−0.67	−0.15	0.00
$\Delta E_{ads}(C2)$	−1.20	−0.82	−0.79	−1.24
$E_{ads}(C_3H_4)$	−1.57	−1.19	−0.59	−0.68
$E_{ads}(C_3H_6)$	−0.60	−0.43	−0.01	0.69
$\Delta E_{ads}(C3)$	−0.97	−0.76	−0.58	−1.37

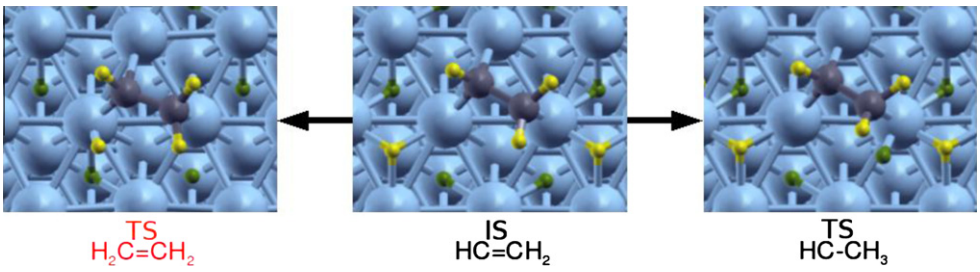

Fig. 8. Schematic representation for the hydrogenation of vinyl (IS) on the palladium hydride phases. Left: transition state from a surface H atom to the formation of ethene (TS $H_2C{=}CH_2$). Right: transition state for the formation of ethylidene with a subsurface H atom (TS $HC{-}CH_3$). Blue spheres represent Pd atoms, yellow surface H atoms, green subsurface H atoms, and gray C atoms. (For interpretation of the references to color in this figure legend, the reader is referred to the web version of this article.)

4.3.2. Thermodynamic factors

The values for the thermodynamic factors for all systems considered in the present work are reported in Table 1. According to this, the most effective model catalysts to obtain a good selectivity towards the double bond are by order of magnitude: CO, then hydrides, carbides, and the most unselective system is the clean surface. Clearly, this is not the case if hydrides are present. Hydride formation produces over-hydrogenated moieties even if the thermodynamic factor is more favorable than for the clean surface. This is due to the presence of new active H species indicated in Fig. 8 that opens a new path in the over-hydrogenation route. Therefore, we stress that the thermodynamic factor can only be considered as a reliable selectivity descriptor provided that the active species are preserved.

4.3.3. Brønsted–Evans–Polanyi relationships

To compile all the results concerning the kinetic parameters for all the reactions in Fig. 7, we have plotted the corresponding Brønsted–Evans–Polanyi relationships (BEP) for C–H dissociation in all the model structures for both C2 and C3 (Fig. 9). Dehydrogenation steps of ethene derivatives on Pd have been found to follow this kind of linear relationships independently of the degree of unsaturation of the hydrocarbon [36]. The present results extend the use of such relationships to different carbon numbers and to all the Pd-derived substrates included in the calculations, *i.e.*, clean surface, hydrides, carbides, and CO-covered surfaces. Remarkably, no individual fitting (either by carbon number or by the state of the catalysts) finds a better correlation than including all data. The success of the present BEP linear relationship is likely to be related to the small ensemble needed for the dehydrogenation reaction: in all transition steps, the H atom is activated to an on-top Pd position.

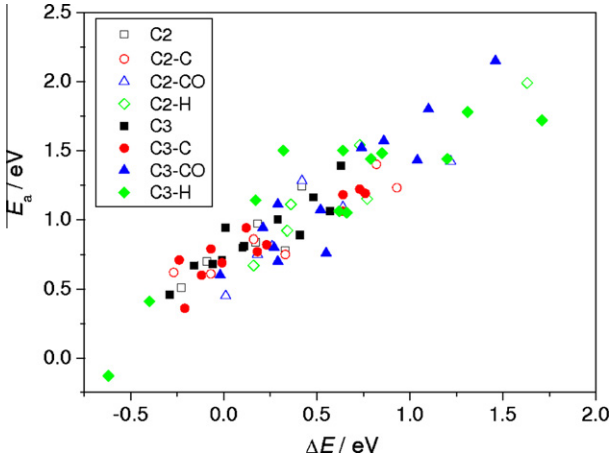

Fig. 9. Brønsted–Evans–Polanyi relationship for the dehydrogenation of C2 and C3 compounds on the clean, carbide, hydride, and CO-covered Pd models. Ethyne (propyne) and the derived products are represented by open (solid) symbols. The regression equation is: $E_a = 0.78\Delta E + 0.71$; $r = 0.90$.

4.3.4. Oligomerization

We discuss first the oligomer formation with ethyne. The initial, transition, and final states are shown in Fig. S3 of the Supplementary material. On the clean surface, the barrier for oligomerization is 1.38 eV. However, if very dense alkyne layers exist, the barrier could be reduced down to 0.86 eV. In the presence of carbides, the reaction barriers are different depending on the local configuration; however, the C–C barrier increases up to 1.71 or 1.99 eV depending if the carbide is along the oligomerization path or farther away from it. Oligomerization is energetically eased in the presence of CO, 0.91 eV, due to both the reduction in the reactants binding energy and the smaller steric hindrance in the final structure. Instead, the coupling barrier is higher on the palladium hydride, 1.52 eV, due to the difficult diffusion. However, for CO and to a lesser extent for hydride, the dense layer formed implies also the isolation of different sites. Thus, there is a geometric contribution that preferentially inhibits oligomer formation due to reduction in the effective ensembles and blocked diffusion. In addition, C–C coupling from vinyl to ethyne shows a smaller barrier than the ethyne–ethyne coupling, 1.19 eV (vs. 1.38 eV), which means that partially hydrogenated molecules are more energetically prone to undergo oligomerization. Finally, CO can also react to the alkyne leading to HC═CH–CO. The barrier for this process is 1.40 eV, hence incorporation of CO to the oligomer cannot be discarded at all.

In general, the C–C coupling barrier is higher for C3 than for C2. This explains, at least partially, why lower oligomer selectivities are found for propyne. In the C3 case, different possibilities for the coupling exist: head-to-head, head-to-tail, and tail-to-tail. We have considered the second option since it is statistically more likely. C–C formation on the clean surface displays a barrier of 1.67 eV. As in the case of ethyne, this barrier is larger in the presence of C (1.88 eV) but slightly reduced in the hydride case (1.52 eV). CO decreases the C–C coupling barrier to 1.50 eV.

In summary, CO significantly reduces the size of the ensembles in such a way that independent alkyne adsorption sites can be considered. While the direct CO effect in the alkyne–alkyne coupling is to lower the reaction barrier, a second contribution coming from the close-packed nature of the CO overlayer is more effective reducing the amount of alkyne coupling by isolation. However, a second source of oligomer production, *i.e.*, the coupling of alkynes (or their derivatives) to CO, increases under CO-rich conditions.

4.4. Interplay of phases in selective hydrogenation

In this section, we will comparatively discuss the experimental and modeling results. As summarized in Section 4.1, catalytic tests

were performed on the as-received catalyst, *i.e.*, non-pretreated, and after pretreatment in alkyne, hydrogen, and the reaction mixture. Then, ethyne and propyne hydrogenation were studied in the absence or presence of CO (Figs. 2–5). We have determined the equilibrium state of the surface under the different conditions employed in the experiments. In order to do so, the combination of the binding energies of H, C, C_2H_2, and CO to the surface (Section 4.2) and the pressures of the corresponding gases: H_2, C_2H_2, and CO, are needed as an input to obtain the hydrogen volume uptake (V/V_m) described in Section 3 (Eqs. (1)–(3)). The derivation of the equations and the data required are summarized in Figs. S4–S6 and Table S2 in Supplementary material. Two different equilibrium diagrams representing the hydrogen uptake V/V_m as a function of H_2, C_2H_2, and CO pressures have been constructed to understand the formation of subsurface hydrogen species ($V/V_m > 1$), which is the main responsible for over-hydrogenation. Results are presented in Fig. 10.

A first scenario consists on pretreatments that only involve the alkyne and hydrogen; the calculations can then be compared to experiments on the non-pretreated sample and the pretreatments with alkyne, hydrogen, and reaction mixture. In these cases, only ethyne (propyne) and hydrogen compete for the formation of carbide and hydride structures. In Fig. 10, $V/V_m > 1$ indicates that the subsurface hydride is being formed. The points corresponding to the experiments in Section 4.1 are indicated in the figure by a red segment. Therefore, we can assign the experiments to H-rich or H-lean regions. Under alkyne pretreatment, carbides can be formed. This implies that full hydrogen coverage is possible but carbides block the formation of subsurface hydrogen species, see Fig. 10a. As pointed out in Section 4.2, the formation of the carbide is strongly dominated by the kinetic aspects of hydrocarbon dissociation. Due to the kinetic control, only experiments in which the pretreatment was performed with alkyne would be likely to generate the carbide layer. Since carbides are formed in the regions close to the steps, mainly these defects and their surroundings (at least 5 Å around the defect) would be H-lean. In regions where carbides cannot be formed (either far away from steps or when lower chemical potential substrates are employed, *i.e.*, propyne and other C3+, see Supplementary Fig. S7, unselective-subsurface hydride species can appear. On the contrary, under hydrogen pretreatment, the hydride would be generated, and carbide formation would be hindered by the presence of H in subsurface sites. According to the phase descriptions and the kinetic studies in Section 4.3, the carbide layer formed is more selective towards the alkene than any of the other phases (see Fig. 5). Over-hydrogenation leads to the alkane as the major product in three cases: hydrogen pretreatment, no pretreatment, and reaction mixture pretreatment (cases (1), (3), and (4) in Fig. 5).

Since the carbide is only effectively formed to a large extent in ethyne pure conditions, in Fig. 10b, we illustrate the interplay between H_2 and CO to understand the effect of the latter on the formation of subsurface hydrogen. In this case, the control variables are the partial pressures of H_2 and CO. Under extremely low CO coverages, V/V_m is larger than 1 indicating the formation of the hydride. But if CO is increased, the equilibrium structure shows a total amount of hydrogen that is not enough to form a full H monolayer on the surface, and no subsurface hydrogen can be formed. From our results, CO enhances alkene production due to the suppression of subsurface H; reduces the total amount of surface hydrogen; improves the thermodynamic control of the alkyne–alkene pair (see Table 1); and isolates the reacting molecules that can not couple to generate oligomers. However, CO could be incorporated in the oligomer.

A summary of the different scenarios that can occur under different reaction conditions is shown in Fig. 11. Initially, more or less clean palladium surfaces are present, Fig. 11a. Carbon impurities coming from hydrocarbon dissociation can appear in the regions near defective areas, Fig. 11b, depleting H coverages from these areas. However, carbide formation depends strongly on the feed hydrogen:alkyne ratio and is kinetically controlled. Thus, it seems unlikely that large particles could form a uniform, selective carbide layer. From an industrial point of view, such catalyst is not robust

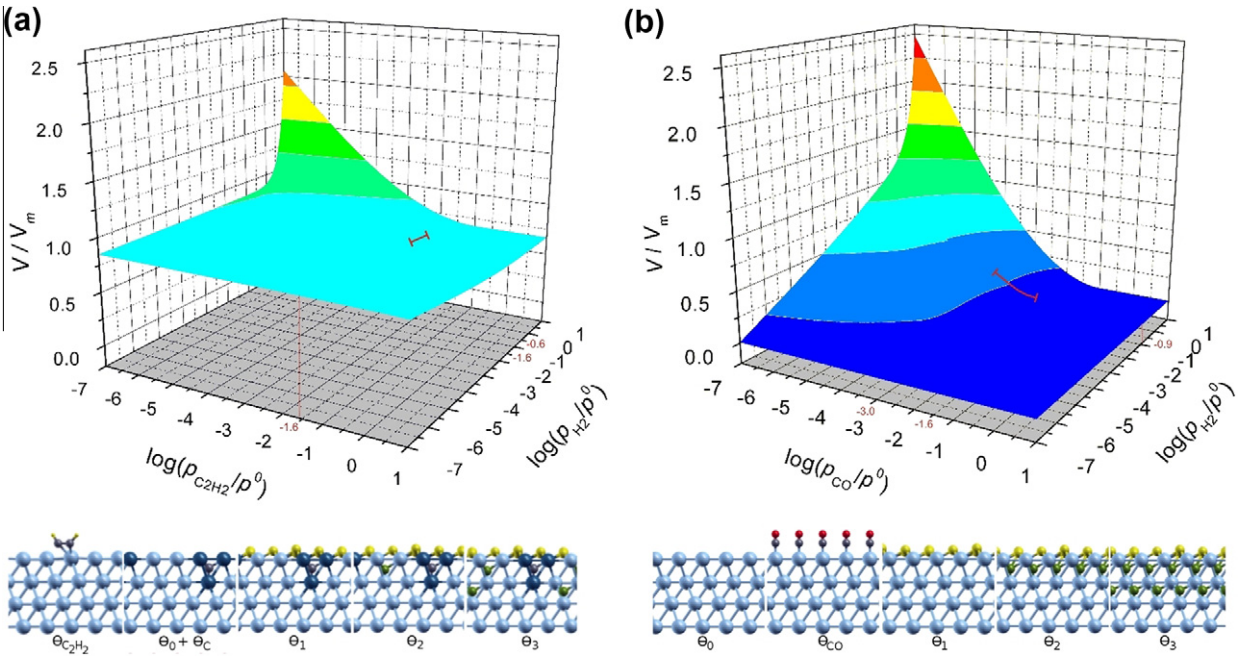

Fig. 10. Hydrogen uptake, V/V_m, of Pd as a function of the relative alkyne–hydrogen–CO pressures at 350 K. (a) Palladium in ethyne–hydrogen mixtures and (b) palladium in CO–H_2 mixtures. The lower panels schematically represent the clean surface θ_0; carbide C, C_2H_2 or CO coverages, θ_C, θ_{C2H2}, and θ_{CO}; and multilayer H adsorption, θ_i. Blue spheres represent Pd, yellow H, gray C and red O. Darker blue denotes Pd atoms in contact with carbon impurities. The red segments in the figure indicate the region where experiments were performed. (For interpretation of the references to color in this figure legend, the reader is referred to the web version of this article.)

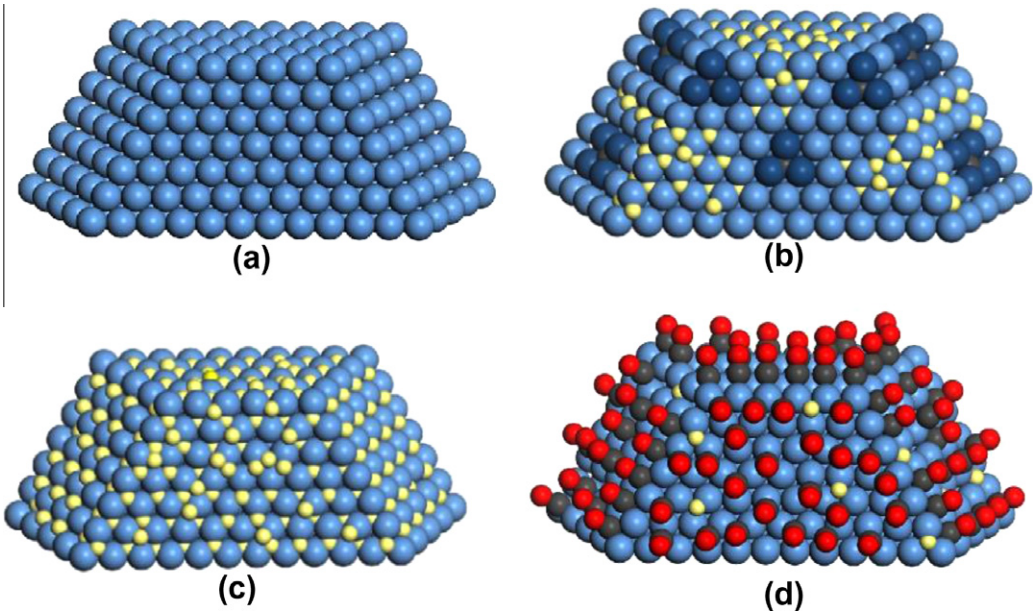

Fig. 11. Schematic representation of the different possible structures under different reaction feeds: (a) clean particle, (b) carbide formation, (c) hydride formation, (d) CO-containing feeds. Same color code as in Fig. 10.

enough since selectivity will depend on the narrow H_2:alkyne window observed in Fig. 1. In fact, there is a spatio-temporal dependence of the carbide–hydride palladium phases during the hydrogenation reaction, Fig. 11b and c. A clear example on the dependence of the history of the samples can be found in the experiments in Figs. 1 and 5. Under the same H_2:alkyne conditions, two different ethene selectivities are found, *ca.* 18% in Fig. 1 and *ca.* 5% in Fig. 5. Indeed, while the catalyst in Fig. 5 was fresh, the corresponding for Fig. 1 was already on stream with a H_2:alkyne ratio of 1 for 2 h. In addition, the dynamics of the hydride phase respond to different external conditions providing very different outlet products with small H_2:alkyne ratio variations. It is even likely that due to this flexibility, different regions of the catalyst are responsible for the generation of different products. If this were the case, the extension of the hydride would control over-hydrogenation products, while alkene products would be derived from the carbide region. The situation is even worse for front-end hydrogenation, where H_2:alkyne ration goes from 10 to 25 but it can be as large as 100. Then, the control *via* the formation of carbides is far too weak to be employed under such extreme conditions. Industrially, in order to have a control on the selectivity in front-end hydrogenation, the CO concentration is varied between 0.15 and 0.5 vol.%. According to our models, CO forms a uniform, homogeneous control layer that displaces both the hydride and the carbide, which results in a robust way of controlling the surface and near-surface Pd catalyst state, Fig. 11d. This dense CO blanket could generate vacancies where the partial hydrogenation reaction can take place. This opens a wide operation window, where the relative H_2:alkyne ratio at which the catalyst might be active and selective is enlarged by several orders of magnitude, see Figs. 2–4. Thus, CO resets the system by setting up a completely new scenario, which is robust in the sense that it shows a moderate dependence on the feed alkyne:H_2 ratio.

5. Conclusions

We have studied the selective hydrogenation of alkynes (ethyne and propyne) on differently pretreated catalysts with and without the presence of CO as a selectivity enhancer. We have identified the narrow H_2:alkyne window that controls the selective production of the desired alkene products (H_2:alkyne = 1–1.7), in the absence of CO. Under this H-poor regime, oligomers are the major competitive route that diminishes the overall alkene yield. Pretreatment under ethyne-only conditions can improve alkene selectivity; however, the effect disappears under other possible pretreatments. Calculations suggest that carbides are likely formed from the steps and diffuse towards the center of the Pd particles. Thus, the formation of this phase is kinetically controlled by the barriers at the step and the number of empty sites. In addition, near-surface positions are energetically more favored for these impurities, and both penetration to the bulk of the particle and formation of dense carbide structures are energetically unfavorable. At higher H_2:alkyne ratio (front-end conditions), the formation of PdH occurs, switching the reaction selectivity towards the production of alkanes. The hydride is easily formed and reversible since charging of the deep Pd layers depends on the full occupation of the surface layer, and both H_2 dissociation and H penetration are rather easy. The high unselective character of the hydride phase is clearly supported in the calculations by the high activity found for nascent H atoms emerging from subsurface positions. The addition of CO shows remarkable effects even at very low concentrations and high H_2:alkyne ratios. CO forms a dense blanket that covers the Pd surface, improves the thermodynamic factor, reduces the amount of available H on the surface and the formation of subsurface H species, and shrinks the size of active ensembles. If carbides are present, they are moved away from the near-surface region. In a way, CO presence overwrites the previous state of the system leading an efficient way to maximize the alkene selectivity over Pd-containing systems.

Acknowledgments

This work was funded by the MICINN (CTQ2006-01562/PPQ, CTQ2006-00464/BQU, CTQ2009-07553/BQU, CTQ2009-09824/PPQ, and Consolider-Ingenio 2010 Grant CSD2006-0003), the Catalan Government (2009-SGR-461, 2009-SGR-259) and the ICIQ Foundation. BSC-RES is acknowledged for providing generous computational resources. We would like to thank Prof. Jens K. Nørskov for stimulating discussions.

Appendix A. Supplementary material

Supplementary data associated with this article can be found, in the online version, at doi:10.1016/j.jcat.2010.04.018.

References

[1] G.A. Somorjai, Y.G. Borodko, Catal. Lett. 76 (2001) 1.
[2] D. Teschner, J. Borsodi, A. Wootsch, Z. Révay, M. Hävecker, A. Knop-Gericke, S.D. Jackson, R. Schlögl, Science 320 (2008) 86.
[3] F. Studt, F. Abild-Pedersen, T. Bligaard, R.Z. Sorensen, C.H. Christensen, J.K. Nørskov, Science 320 (2008) 1320.
[4] A. Molnár, A. Sárkány, M. Varga, J. Mol. Catal. A: Chem. 173 (2001) 185. and references therein.
[5] G.C. Bond, Metal-Catalysed Reactions of Hydrocarbons, Springer, New York, 2005. p. 395.
[6] M.L. Derrien, in: L. Červený (Ed.), Catalytic Hydrogenation, Stud. Surf. Sci. Catal., vol. 27, Elsevier, Amsterdam, 1986, p. 613.
[7] D. Teschner, Z. Revay, J. Borsodi, M. Hävecker, A. Knop-Gericke, R. Schlögl, D. Milroy, S.D. Jackson, D. Torres, P. Sautet, Angew. Chem. Int. Ed. 47 (2008) 9274.
[8] N.N. Greenwood, A. Earnshaw, Chemistry of the elements, second ed., Elsevier, 2008. p. 1150, and references therein.
[9] A. Borodziński, G.C. Bond, Catal. Rev. Sci. Eng. 48 (2006) 91.
[10] A.D. Johnson, S.P. Daley, A.L. Utz, S.T. Ceyer, Science 257 (1992) 223.
[11] H. Molero, B.F. Bartlett, W.T. Tysoe, J. Catal. 181 (1999) 49.
[12] K. Kovnir, J. Osswald, M. Armbrüster, D. Teschner, G. Weinberg, U. Wild, A. Knop-Gericke, T. Ressler, Y. Grin, R. Schlögl, J. Catal. 264 (2009) 93.
[13] W. Buchele, H. Roos, H. Wanjek, H.J. Muller, Catal. Today 30 (1996) 33.
[14] P.A. Sheth, M. Neurock, C.M. Smith, J. Phys. Chem. B 107 (2003) 2009.
[15] D.H. Mei, P.A. Sheth, M. Neurock, C.M. Smith, J. Catal. 242 (2006) 1.
[16] F. Studt, F. Abild-Pedersen, T. Bligaard, R.Z. Sørensen, C.H. Christensen, J.K. Nørskov, Angew. Chem. Int. Ed. 47 (2008) 9299.
[17] Y. Segura, N. Lopez, J. Pérez-Ramírez, J. Catal. 247 (2007) 383.
[18] B. Bridier, N. Lopez, J. Pérez-Ramírez, J. Catal. 269 (2010) 80.
[19] B. Bridier, J. Perez-Ramirez, J. Am. Chem. Soc. 132 (2010) 4321.
[20] D.H. Mei, M. Neurock, C.M. Smith, J. Catal. 268 (2009) 181.
[21] N. Lopez, B. Bridier, J. Pérez-Ramírez, J. Phys. Chem. C 112 (2008) 9346.
[22] G. Kresse, J. Hafner, Phys. Rev. B 47 (1993) 558.
[23] R.W.G. Wyckoff, Crystal Structures, Interscience, New York, 1965.
[24] A. Borodziński, G.C. Bond, Catal. Rev. Sci. Eng. 50 (2008) 379.
[25] H.J. Monkhorst, J.D. Pack, Phys. Rev. B 13 (1976) 5188.
[26] J.P. Perdew, J.A. Chevary, S.H. Vosko, K.A. Jackson, M.R. Pederson, D.J. Singh, C. Fiolhais, Phys. Rev. B 46 (1992) 6671.
[27] P.E. Blöchl, Phys. Rev. B 50 (1994) 17953.
[28] G. Henkelman, B.P. Uberuaga, H. Jonsson, J. Chem. Phys. 113 (2000) 9901.
[29] J. Greeley, W.P. Krekelberg, M. Mavrikakis, Angew. Chem. Int. Ed. 43 (2004) 4296.
[30] S. Brunauer, P.H. Emmett, E. Teller, J. Am. Chem. Soc. 60 (1938) 309.
[31] X.G. Wang, A. Chaka, M. Scheffler, Phys. Rev. Lett. 84 (2000) 3650.
[32] T. Mitsui, M.K. Rose, E. Fomin, D.F. Ogletree, M. Salmeron, Nature 422 (2003) 705.
[33] N. Lopez, Z. Łodziana, F. Illas, M. Salmeron, Phys. Rev. Lett. 93 (2004) 146103.
[34] M.K. Rose, A. Borg, T. Mitsui, D.F. Ogletree, M. Salmeron, J. Chem. Phys. 115 (2001) 10927.
[35] L. Gracia, M. Calatayud, J. Andres, C. Minot, M. Salmeron, Phys. Rev. B 71 (2005) 033407.
[36] J. Andersin, N. Lopez, K. Honkala, J. Phys. Chem. C 113 (2009) 8278.
[37] L. Nykanen, J . Andersin, K. Honkala, Phys. Rev. B 81 (2010) 075417.
[38] M. Ruta, N. Semagina, L. Kiwi-Minsker, J. Phys. Chem. C 112 (2008) 13635.
[39] S.B. Ziemecki, G.A. Jones, D.G. Swartzfager, J. Less-Common. Metals 131 (1987) 15.
[40] D. Loffreda, D. Simon, P. Sautet, Surf. Sci. 425 (1999) 68.
[41] K. Honkala, P. Pirila, K. Laasonen, Surf. Sci. 489 (2001) 72.
[42] M.K. Rose, T. Mitsui, J. Dunphy, A. Brog, D.F. Ogletree, M. Salmeron, P. Sautet, Surf. Sci. 512 (2002) 48.
[43] J. Horiuti, M. Polanyi, Trans. Faraday Soc. 30 (1934) 1164.